Ain Shams Engineering Journal (2016) 7, 729–740

Ain Shams University

Ain Shams Engineering Journal

www.elsevier.com/locate/asej
www.sciencedirect.com

ELECTRICAL ENGINEERING

Neural network-based sensorless direct power control of permanent magnet synchronous motor

Mahdi Zolfaghari [a], Seyed Abbas Taher [b,*], David Vindel Munuz [c]

[a] Department of Electrical Engineering, Amirkabir University, Tehran, Iran
[b] Department of Electrical Engineering, University of Kashan, Kashan, Iran
[c] Department of Energy and Environment, Chalmers University of Technology, Sweden

Received 28 January 2015; revised 11 November 2015; accepted 8 January 2016
Available online 1 February 2016

KEYWORDS

PMSM;
Direct power control;
Artificial neural network;
MRAS

Abstract In this paper, a sensorless permanent magnet synchronous motor (PMSM) drive was presented based on direct power control (DPC) technique. To estimate the rotor's position and speed of PMSM, a drastic sensorless strategy was developed according to artificial neural network (ANN) to reduce the cost of the drive and enhance the reliability. The proposed sensorless scheme was an innovative model reference adaptive system (MRAS) speed observer for DPC control PMSM drives. The suggested MRAS speed observer employed the current model as an adaptive model. The ANN was then designed and trained online by employing a back propagation network (BPN) algorithm. Performance of the proposed strategy was adopted using simulation analysis. The results showed the fast dynamic response, low ripples in motor's currents, power, and electromagnetic torque, as well as good performance in tracking speed and power references.

1. Introduction

Recently, PMSMs have received more interest, since they are more efficient and cost-effective and have an appropriate speed control range and reduced maintenance requirements [1,2]. For PMSM drives, several control strategies have been reported in the literature [1,3]. The well-known technique, direct torque control (DTC), is now being adopted by the industry. However, DTC still has some drawbacks such as relatively high ripples in flux and torque [4,5]. Also, the switching frequency of the inverter is not constant for a DTC without vector control method and changes with rotor speed, load torque, and bandwidth of the two hysteresis controllers. Direct power control (DPC) is a control technique which, without using current loops, directly selects output voltage vector states based on the power and flux errors using hysteresis controllers. In this respect, it is the same as DTC. Similar to DTC, DPC is a stator flux-based control technique with the advantages of robustness and fast control [6]. DPC has the following advantages: simpler voltage and power estimation algorithm, easy implementation of the unbalanced and distorted line voltage compensation to obtain sinusoidal currents (low THD),

* Corresponding author at: Department of Electrical Engineering, University of Kashan, 6 km Ravand Road, Kashan, Iran. Tel./fax: +98 3615559930.
E-mail address: sataher@kashanu.ac.ir (S.A. Taher).
Peer review under responsibility of Ain Shams University.

Production and hosting by Elsevier

http://dx.doi.org/10.1016/j.asej.2016.01.002

excellent dynamics, and no need for coordinate transformation [7].

Basically, DPC is applied to generators. In [8], the conventional DTC scheme for inducing motor drives was extended to directly control the active power (DPC) delivered to an active load by a wind turbine driven squirrel cage induction generator (SCIG). The SCIG was interfaced to the load through an AC–DC converter (PWM rectifier). The goal of this control system was to maintain the DC bus voltage at a constant value independent from the variations of the load. In [9], for a doubly fed induction generator (DFIG), an algorithm was developed for the independent control of active and reactive powers with high dynamic response. The instantaneous switching state of the rotor side converter (RSC) was determined based on the active and reactive powers measured in the stator circuit. Measurements were carried out in one terminal of the machine, whereas the switching action was performed in another terminal. The directly controlled quantities were the stator active and reactive powers. A new adaptive control strategy for a wind energy conversion system based on a permanent magnet synchronous generator and a pulse-width modulated current source converter were introduced in [10]. This conversion system was a good alternative because of its high efficiency and reliability. Electrolytic capacitors were not required in this type of converter and the voltage in the DC-link as well as the generated reactive power could be dynamically modified according to wind velocity, being even negative if required. However, it was challenging from the control and stability standpoints [11,12].

In [13], a combined vector and direct power control (CVDPC) was proposed for the RSC of DFIGs. The control system was based on a direct current control by selecting appropriate voltage vectors from a switching table. In fact, the CVDPC enjoyed from the benefits of vector control (VC) and DPC in a compacted control system. Its benefits, in comparison with VC, included fast dynamic response, robustness against variation of machine parameters, lower computation, and simple implementation [14–16]. A direct rotor current mode control (CMC) was suggested in [17] for the RSC of induction generators, which was aimed to improve the transient response in relation to the dynamic performance achieved by the conventional (indirect) CMC. A simple method for achieving the predictive direct power control (PDPC) for DFIG-based wind energy conversion systems was proposed in [18]. This approach was able to operate at low switching frequency and provide excellent steady-state and dynamic performances, which were useful for high-power wind energy applications. Three vectors were selected and applied during one control period to reduce both active and reactive power ripples. Compared to the prior three-vectors-based art using two switching tables, the approach only needed one unified switching table to obtain the three vectors [19,20]. Nowadays, it has been tried to employ DPC to control electrical motors instead of DTC techniques due to the problems of torque estimation and dependence on motor parameters in DTC. Thus, DPC technique relishes all the advantages of DTC such as fast dynamics and implementation ease without having its problems.

In machine learning and cognitive science, artificial neural networks (ANNs) are a family of statistical learning algorithms inspired by biological neural networks (the central nervous systems of animals, in particular the brain) and are used

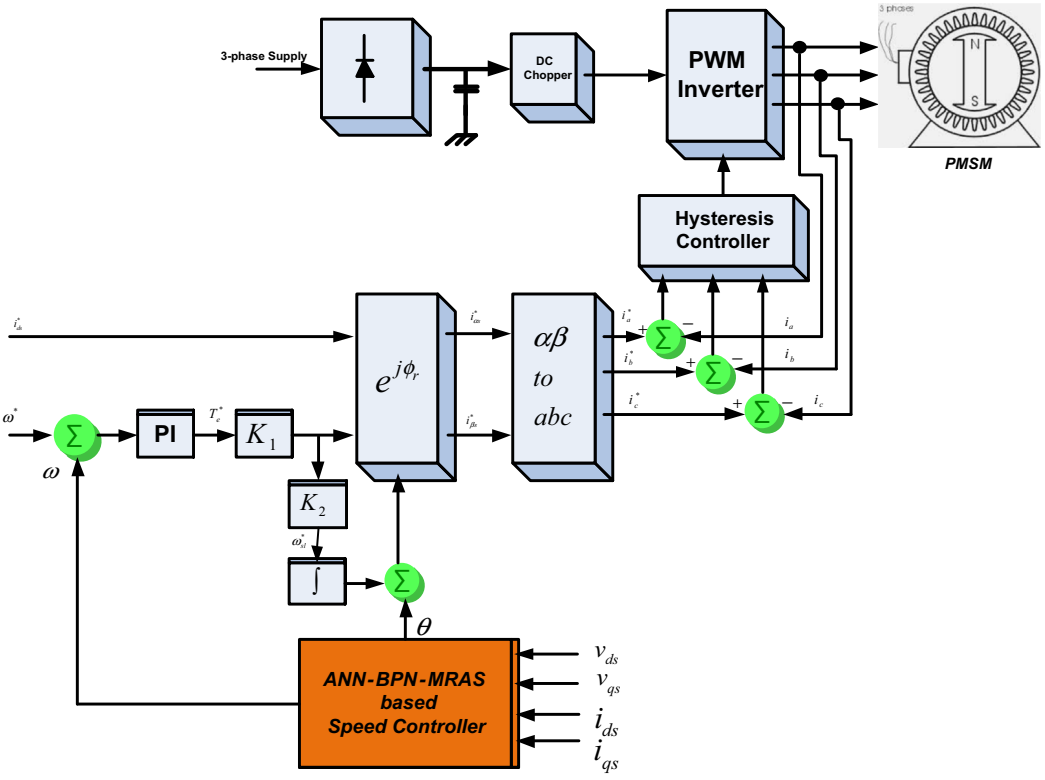

Figure 1 Overall diagram of sensorless control of PMSM drive using the proposed ANN-BPN-MRAS based speed estimator.

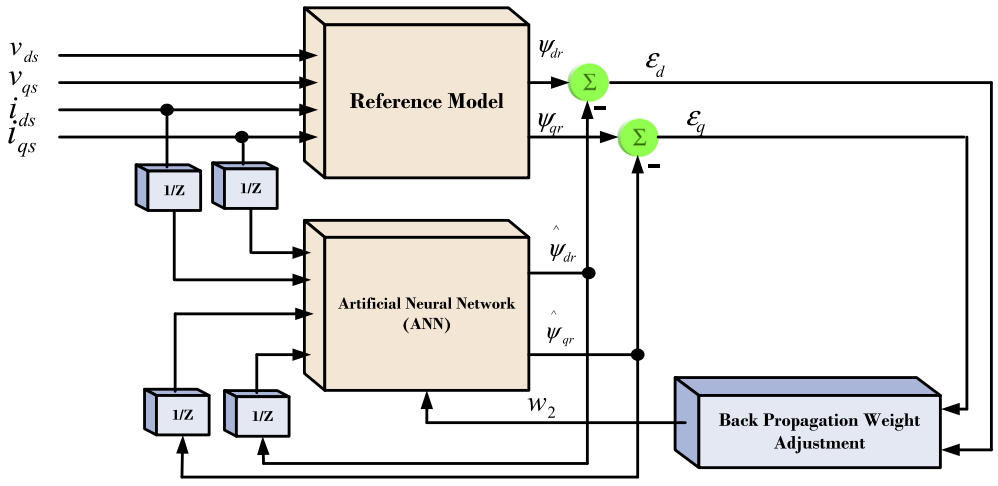

Figure 2 The proposed speed estimator based on MRAS including an ANN.

to estimate or approximate functions that can depend on a large number of inputs and are generally unknown [22]. ANNs are generally presented as systems of interconnected "neurons" which can compute values from inputs and are capable of machine learning as well as pattern recognition, thanks to their adaptive nature. Like other machine learning methods – systems that learn from data, neural networks have been used to solve a wide variety of tasks that are hard to solve using ordinary rule-based programming, including computer vision and speech recognition.

In the present study, a sensorless PMSM drive was presented based on DPC technique, in which the motor speed was estimated using an ANN-based MRAS speed estimator. The proposed control scheme was a model reference adaptive system (MRAS) speed observer for DPC control PMSM drives. The suggested MRAS speed observer employed the current model as an adaptive model. The ANN was then designed and trained online by employing a back propagation network (BPN) algorithm. The simulation and experimental results were presented to verify the performance of the proposed PMSM drive.

2. Dynamic model of PMSM

Electrical drives with PMSMs have found a wide implementation in different fields of the present day society, whereas vector control has become the state of the art method of the a.c. drive control. Drive structure usually involves an a.c. machine equipped with sensors, a microcontroller, and a PWM inverter. Based on data received from position (θ_{means}) and current sensors, microcontroller generates pulse width modulated voltage patterns, which, amplified by PWM inverter, drive PMSM.

Model of a sinusoidal PMSM can be described in the rotor d–q reference frame by the following equations [1,12]:

$$\begin{aligned} v_d &= Ri_d + L_d\frac{di_d}{dt} - L_q P_p \omega i_q \\ v_q &= Ri_q + L_q\frac{di_q}{dt} + L_d P_p \omega i_d + P_p \omega \lambda_{PM} \\ T_m &= \frac{3}{2}P_p[\lambda_{PM} i_q + (L_d - L_q) i_d i_q] \\ \frac{d\omega}{dt} &= \frac{1}{J}(T_m - T_L - F\omega) \\ \frac{d\theta}{dt} &= \omega \end{aligned} \tag{1}$$

where v_d, v_q are the stator voltages in the rotor reference frame, i_d, i_q are the stator currents in the rotor reference frame, R is the stator phase resistance, L_d, L_q are the machine inductances, respectively, along direct quadrature axis, P_p is the number of motor pole pairs, λ_{PM} is the flux generated by permanent magnets, T_m is the electromagnetic torque, T_L is the load torque, F is the viscous friction coefficient, J is the moment of inertia of all rotating masses, ω is the instantaneous angular speed, and θ is the instantaneous angular position.

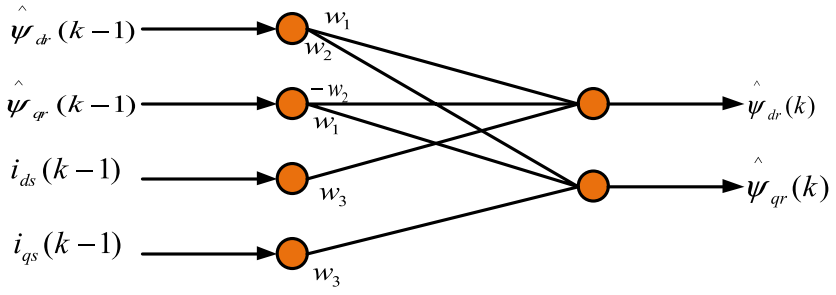

Figure 3 ANN pattern for rotor flux estimation.

Table 1 On and off states and the corresponding outputs of a three-phase VSI.

State	S_a	S_b	S_c	u_a/U_{dc}	u_b/U_{dc}	u_c/U_{dc}	u_{ab}	u_{bc}	u_{ca}	u_α/U_{dc}	u_β/U_{dc}
$\underline{u}_0$	0	0	0	0	0	0	0	0	0	0	0
$\underline{u}_5$	0	0	1	$-1/3$	$-1/3$	$2/3$	0	-1	1	$-1/3$	$-1/\sqrt{3}$
$\underline{u}_3$	0	1	0	$-1/3$	$2/3$	$-1/3$	-1	1	0	$-1/3$	$1/\sqrt{3}$
$\underline{u}_4$	0	1	1	$-2/3$	$1/3$	$1/3$	-1	0	1	$-2/3$	0
$\underline{u}_1$	1	0	0	$2/3$	$-1/3$	$-1/3$	1	0	-1	$2/3$	0
$\underline{u}_6$	1	0	1	$1/3$	$-2/3$	$1/3$	1	-1	0	$1/3$	$-1/\sqrt{3}$
$\underline{u}_2$	1	1	0	$1/3$	$1/3$	$-2/3$	0	1	-1	$1/3$	$1/\sqrt{3}$
$\underline{u}_7$	1	1	1	0	0	0	0	0	0	0	0

3. Proposed PMSM control scheme

3.1. Speed estimation

A complete block diagram of the proposed ANN-MRAS-based sensorless control of PMSM drive is shown in Fig. 1. MRAS scheme is less complex and more effective. The MRAS approach uses two models. The model that does not involve the quantity to be estimated is considered the reference model. The model that has the quantity to be estimated is considered the adaptive model (or adjustable model). The output of the adaptive model is compared to that of the reference model and the difference is used to drive a suitable adaptive mechanism whose output is the quantity to be estimated (the rotor speed). The adaptive mechanism should be designed to assure the stability of the control system. The MRAS uses redundancy of two-machine model of different structures that estimate the same state variables. Both models are referred to in the stationary reference frame and the output of a reference model is compared to the output of an adjustable or adaptive model until the errors between the two models vanish to zero. With the correct value of rotor speed, the fluxes determined from the two models should match. An adaptation algorithm can be used to tune the speed value until the two flux values match.

In MRAS technique, some state variables, x_d, x_q (e.g. rotor flux-linkage component, e_d, e_q, etc.) of the machine (obtained by measured quantities, e.g. stator voltages and currents) are estimated in a reference model and then compared with the state variables $\hat{x}_d, \hat{x}_q$ estimated by an adaptive model. The

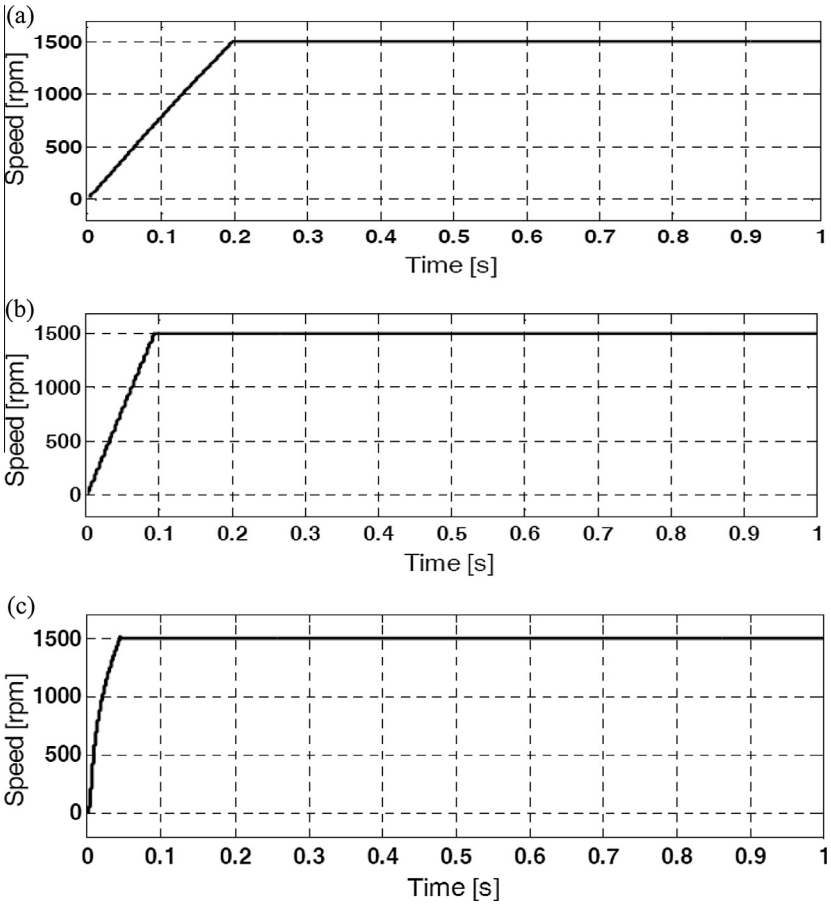

Figure 4 Response of the speed PMSM motor: (a) dc link current control, (b) DTC, and (c) the proposed DPC scheme.

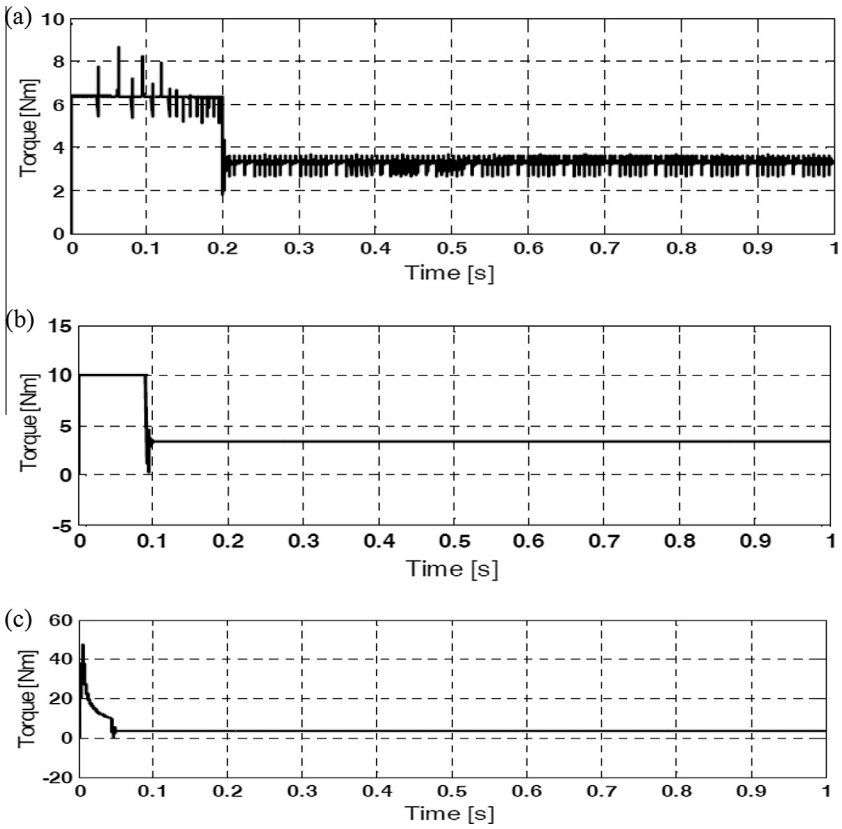

Figure 5 Response of the torque of PMSM motor: (a) dc link current control, (b) DTC, and (c) the proposed DPC scheme.

difference between these state variables is then formulated as a speed tuning signal (ε), which then becomes an input for the adaptation mechanism and outputs the estimated rotor speed ($\hat{\omega}$). Speed estimator using ANN is a part of a MRAS, where ANN takes the role of the adaptive model. ANN contains the adjustable and constant weights and the adjustable weights are proportional to the rotor speed. The adjustable weights are changed by the error between the outputs of the reference and adaptive model. Fig. 2 shows the MRAS-based speed estimation scheme, which contains an ANN with BPN adaptation technique. Outputs of the reference model are the rotor flux linkage components in stationary reference frame, as given by [1,12]:

$$\begin{aligned}\psi_{dr} &= \frac{L_r}{L_m}\left[\int (v_{ds} - R_s i_{ds})dt - L_s i_{ds}\right] \\ \psi_{qr} &= \frac{L_r}{L_m}\left[\int (v_{qs} - R_s i_{qs})dt - L_s i_{qs}\right]\end{aligned} \tag{2}$$

These two equations do not contain the rotor speed and describe the reference model. The equations of adaptive model are given by [1,12]

$$\begin{aligned}\widehat{\psi}_{dr} &= \frac{1}{T_r}\int (L_m i_{ds} - \widehat{\psi}_{dr} - \omega_r T_r \widehat{\psi}_{qr})dt \\ \widehat{\psi}_{qr} &= \frac{1}{T_r}\int (L_m i_{qs} - \widehat{\psi}_{qr} - \omega_r T_r \widehat{\psi}_{dr})dt\end{aligned} \tag{3}$$

It is possible to implement Eqs. (3) and (4) by a two-layer ANN containing weights, $w_1(=1-c), w_2(=\omega_r c T_r = \omega_r T)$ and $w_3(=cL_m)$, where $c = T/T_r$. T, T_r are sampling time and rotor time constant. The variable ANN weight w_2 is proportional to the rotor speed. Using the backward difference method, the equation of adaptive model is given as follows:

$$\begin{aligned}\widehat{\psi}_{dr}(k) &= w_1\widehat{\psi}_{dr}(k-1) - w_2\widehat{\psi}_{qr}(k-1) + w_3 i_{ds}(k-1) \\ \widehat{\psi}_{qr}(k) &= w_1\widehat{\psi}_{qr}(k-1) + w_2\widehat{\psi}_{dr}(k-1) + w_3 i_{qs}(k-1)\end{aligned} \tag{4}$$

which gives the value of rotor flux at the k^{th} sampling instant. These equations can be visualized by the very simple two-layer ANN shown in Fig. 3 [22]. The back propagation algorithm [23] is used in the layered feed-forward ANN. This means that the artificial neurons are organized in layers, their signals are sent "forward", and then the errors are propagated backwards. The network receives inputs by neurons in the input layer and the output of the network is given by the neurons on an output layer.

3.2. Power control

The main issue in DPC is the correct power calculation. If the stator winding loss and core loss are small enough to be neglected, the input electrical power is the same as the electromagnetic power. If the rotational losses are also small and negligible, the electrical input power can be approximated as the mechanical output power. Thus

$$P_{in} \cong P_e = P_{out} \tag{5}$$

where P_{in}, P_e, and P_{out} represent the electrical input power, electromagnetic power, and mechanical output power,

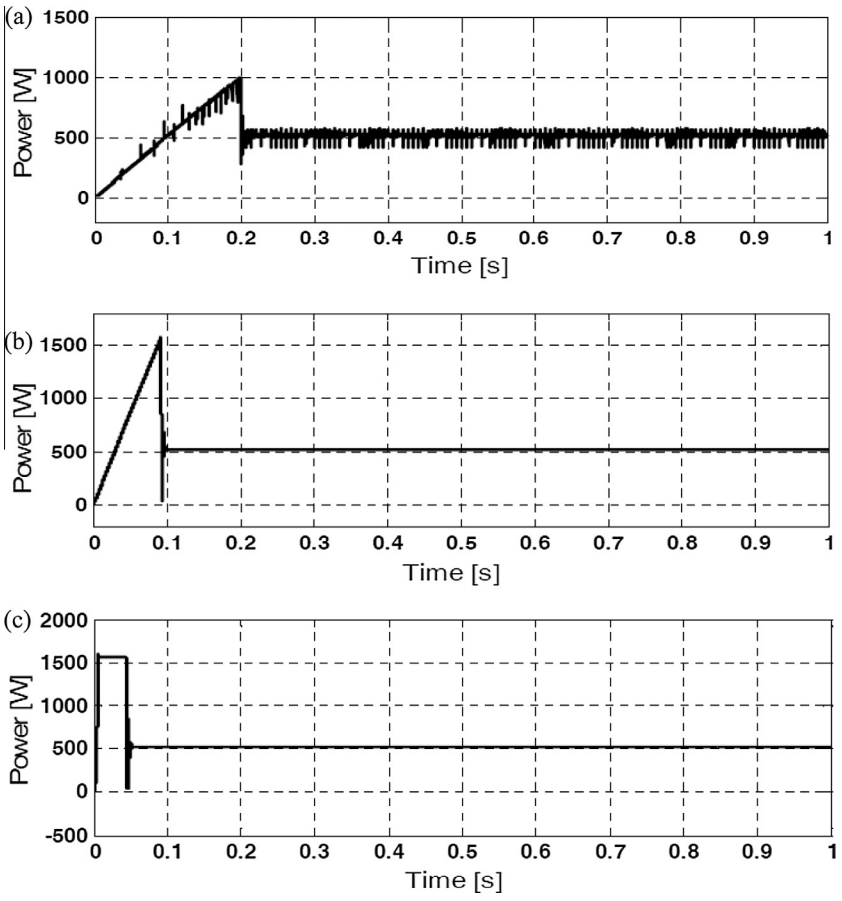

Figure 6 Response of the power of PMSM motor: (a) dc link current control, (b) DTC, and (c) the proposed DPC scheme.

respectively. The mechanical input power can be expressed as follows:

$$P_{out} = T_{em}\frac{\omega_r}{P} \tag{6}$$

The electromagnetic torque of a PMSM in the synchronously rotating d–q reference frame can be expressed as follows [21]:

$$T_{em} = \frac{3P}{4}\left[\left(\frac{dL_{ds}}{d\theta_e}i_{sd} + \frac{d\psi_{rd}}{d\theta_e} - \psi_{sq}\right)i_{sd} + \left(\frac{dL_{dq}}{d\theta_e}i_{sq} + \frac{d\psi_{rq}}{d\theta_e} - \psi_{sd}\right)i_{sq}\right] \tag{7}$$

Substituting the torque in (6) by (7) results in the output power as

$$P_{out} = \frac{3\omega_r}{4}\left[\left(\frac{dL_{ds}}{d\theta_e}i_{sd} + \frac{d\psi_{rd}}{d\theta_e} - \psi_{sq}\right)i_{sd} + \left(\frac{dL_{dq}}{d\theta_e}i_{sq} + \frac{d\psi_{rq}}{d\theta_e} - \psi_{sd}\right)i_{sq}\right] \tag{8}$$

where $\psi_{sd} = L_{sd}i_{sd} + \psi_{rd}$, $\psi_{sq} = L_{sq}i_{sq} + \psi_{rq}$, θ_e is the rotor electrical angle, P is the number of poles, i_{sd}, i_{sq} are d and q-axes currents, L_{ds}, L_{qs} are d and q-axes stator inductances, and $\psi_{rd}, \psi_{rq}, \psi_{sd}$ are d and q-axes rotor and stator flux linkages, respectively.

3.3. Hysteresis controller and PWM inverter

Among the various PWM techniques, the hysteresis band current control is used very often because of its implementation simplicity. Also, besides fast response current loop, the method does not need any knowledge of load parameters. However, the current control with a hysteresis band has the disadvantage that the PWM frequency varies within a band, because peak-to-peak current ripple is required to be controlled at all points of the fundamental frequency wave. The method of adaptive hysteresis-band current control PWM technique, in which the band can be programmed as a function of load to optimize the PWM performance, was described in [3]. The basic implementation of hysteresis current control is based on deriving the switching signals from the comparison of the current error with a fixed tolerance band. This control is based on the comparison of the actual phase current with the tolerance band around the reference current associated with that phase. On the other hand, this type of band control is negatively affected by the phase current interactions which is typical in three-phase systems, which is mainly due to the interference between the commutations of the three phases, since each phase current not only depends on the corresponding phase voltage, but is also affected by the voltage of the other two phases. Depending on load conditions, switching frequency may vary during the fundamental period, resulting in irregular inverter operation. In [4], the authors proposed a new method that

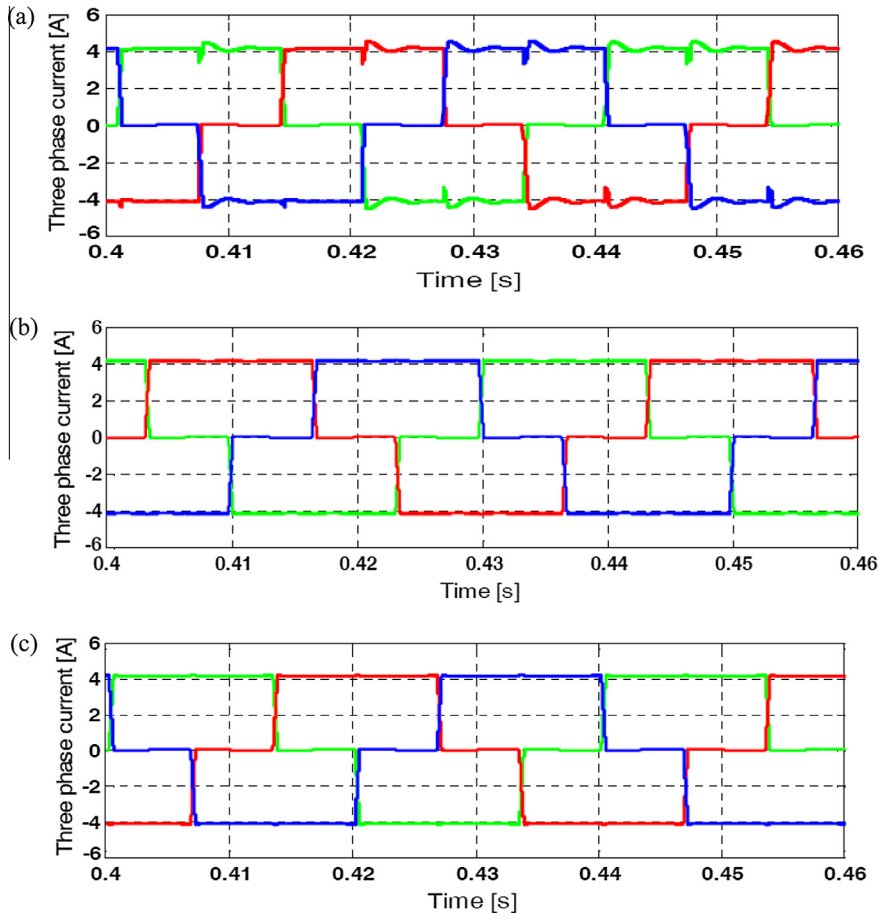

Figure 7 Three phase current of PMSM motor: (a) dc link current control, (b) DTC, and (c) the proposed DPC scheme.

minimized the effect of interference between phases while maintaining the advantages of the hysteresis methods using phase-locked loop (PLL) technique to constrain the inverter switching at fixed predetermined frequency. In this paper, the current control of PWM-VSI was implemented in the stationary (α, β) reference frame. One method was based on space vector control using multilevel hysteresis comparators where the hysteresis band appeared as a hysteresis square. The second method was based on predictive current control where the three hysteresis bands formed a hysteresis hexagon. To describe inverter output voltage and analyze the current control methods, the concept of a complex space vector was applied. This concept provides the possibility of representing three phase quantities (currents or voltages) with one space vector. Eight conduction modes of inverter are possible, i.e. the inverter can apply six nonzero voltage vectors *uk* (k = 1–6) and two zero voltage vectors (k = 0. 7) to the load. The state of switches in inverter legs a; b; c denoted as Sk(Sa; Sb; Sc) corresponds to each vector uk, where for Sa; b; c = 1 the upper switch is on and, for Sa; b; c = 0, the lower switch is on. The switching rules are as follows: due to the DC-link capacitance, the DC voltage must never be interrupted and the distribution of the DC-voltage Udc into the three line-to-line voltages must not depend on the load. According to these rules, one of the upper and one of the lower switches must be closed all the time. There are eight possible combinations of on and off switching states. The combinations and the corresponding phase and line-to-line voltages for each state are given in Table 1 in terms of supplying DC voltage Udc. If we use the transformation from three-phase (a, b, c) into stationary (α, β) coordinate system, then

$$\begin{bmatrix} u_\alpha \\ u_\beta \end{bmatrix} = \begin{bmatrix} \frac{2}{3} & -\frac{1}{3} & -\frac{1}{3} \\ 0 & \frac{1}{\sqrt{3}} & -\frac{1}{\sqrt{3}} \end{bmatrix} \begin{bmatrix} u_a \\ u_b \\ u_c \end{bmatrix} \tag{9}$$

4. Simulation results

In this section, performance of the proposed drive system is evaluated through simulation analysis using MATLAB/SIMULINK [24]. The values of the parameters of PMSM for these simulations are given in Appendix A. Here, three case studies are considered. In the first case, the PMSM using DPC, DTC, and dc link current control method is driven. The response of the proposed PMSM drive to an arbitrary reference power is investigated in the second case. Both aforementioned case studies deal with nonlinear model of the motor. However, the third case analyzes the linearized model of the PMSM.

Case I. Here, the performance of the proposed PMSM drive was extensively compared to DTC and dc link current control schemes. The motor was operating in its normal condition.

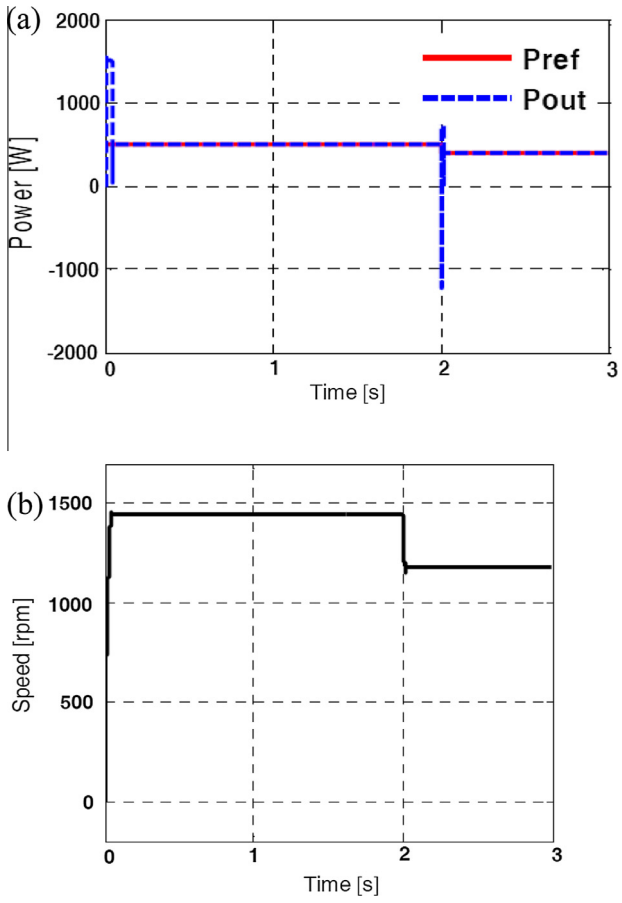

Figure 8 Tracking of the reference power via DPC technique for PMSM: (a) reference power tracking and (b) speed.

The simulation results are shown in Figs. 4–7. As shown in Fig. 4, the response of the speed was good and acceptable in all three methods. However, it is clear that the time to reach the final value in the method of DPC was less than the other methods. The rise time in the speed response of the PMSM using the proposed DPC scheme was the least of all three methods. Figs. 5 and 6 show the response of power and torque of PMSM, respectively. The ripple of power and torque was increased in dc link current method compared to the other method. As shown in Fig. 6, the changes in the power by the proposed DPC lasted shorter than the DTC. The same discussion can be given about the torque. Fig. 7 shows the three-phase current of PMSM, in which DPC and DTC methods were more suitable rectangular than dc link current control.

Case II. In this case, the capability of the PMSM equipped with the proposed DPC control scheme in tracking a reference power was verified. In this part of the simulation, PMSM motor was driven by DPC method. At first, the reference power of 500 W was assumed. Next, the reference power of 400 W was applied at $t = 2$ s. The hysteresis band for the control of power was 5% around the reference value. Waveforms of the generated power and speed are shown in Fig. 8. The power tracking had a good response in transient and steady-state situations. The power followed changing the reference power as well. Decreasing the power decreased the speed of the motor. However, the response of the actual power had overshot, resulting from anti-windup phenomenon that caused the overshot in the response of the speed and power.

Case III. Response of the linearized model of the motor to the proposed control strategy is analyzed in this case. The linearization method is based on quadratic linearization technique and removes the dominant quadratic nonlinearity of the model as well as higher order terms involving the input in the system. A synopsis of the linearization process is given in Appendix A. For more information and definition of other parameters, please see [25–27]. Fig. 9 shows the response of the motor after linearization. As shown, the system has stabilized for the pulse inputs $u_1 = u_2 = 0.1\{u(t) - u(t-1)\}$ where $u(t)$ is

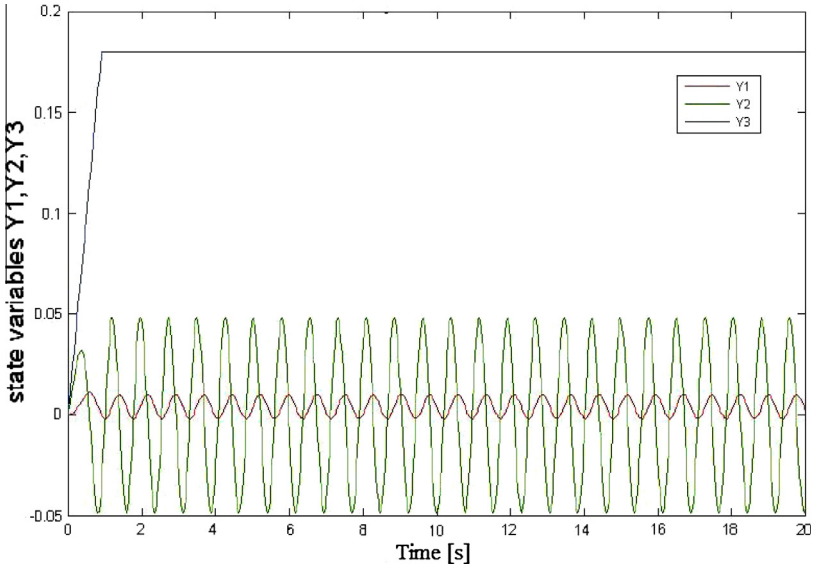

Figure 9 Response of y_1, y_2, y_3 for the linearized system.

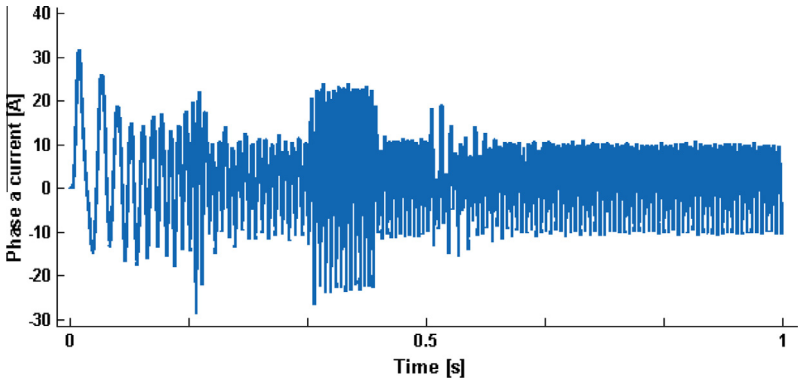

Figure 10 Phase A current of the linearized PMSM equipped with the proposed control strategy.

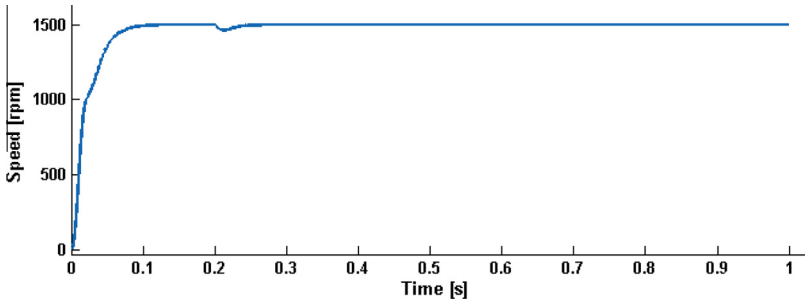

Figure 11 Speed response of the linearized PMSM equipped with the proposed control strategy.

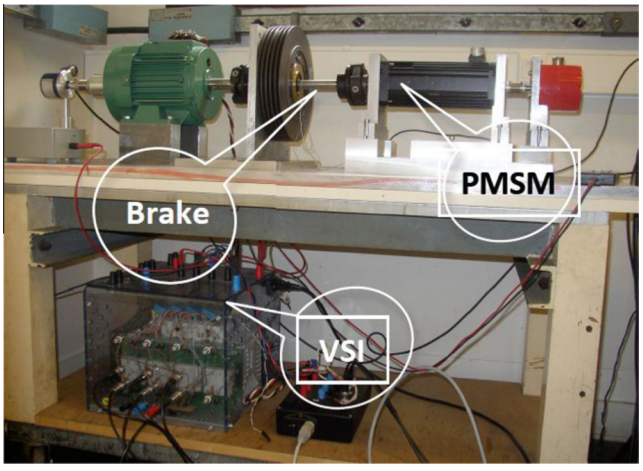

Figure 12 Laboratory test bed.

the unit step function. Here y_1, y_2 are the linearized direct and quadratic currents and x_3 is the angular velocity. Figs. 10 and 11 show the current of phase A and speed response of the linearized model of PMSM equipped with the proposed control strategy. As shown, the machine operates in stable condition.

5. Practical implementation of the PMSM drive system

An experimental system is designed to implement the proposed control scheme of PMSM. Fig. 12 shows the laboratory test bed and Fig. 13 shows a simple schematic diagram of the system. The equipment used in the laboratory setup is listed below:

- Permanent magnet synchronous motor (PMSM).
- Inverter.
- Voltage, current and other measurement equipment.
- dSpace DS1103 control system.
- 24V relay.
- An optocard for over-current protection.
- Various electrical items such as wires, connectors, grounding and so on.

All these equipment are installed and organized in the following way:

- A measurement box that includes the following:
  - DC voltage source that provides the equipment with ± 15 V.
  - Three voltage transducers UMAT2 with three channels for voltage measurements each one.
  - Seven current sensors LEM LA 50-S for current measurements.
  - A resolver-to-digital converter that measures rotor angle and speed.
  - Connector terminals to electrically link different components.
- The inverter box that includes the following:
  - A ± 15 V DC voltage source that supplies the inverter control system.

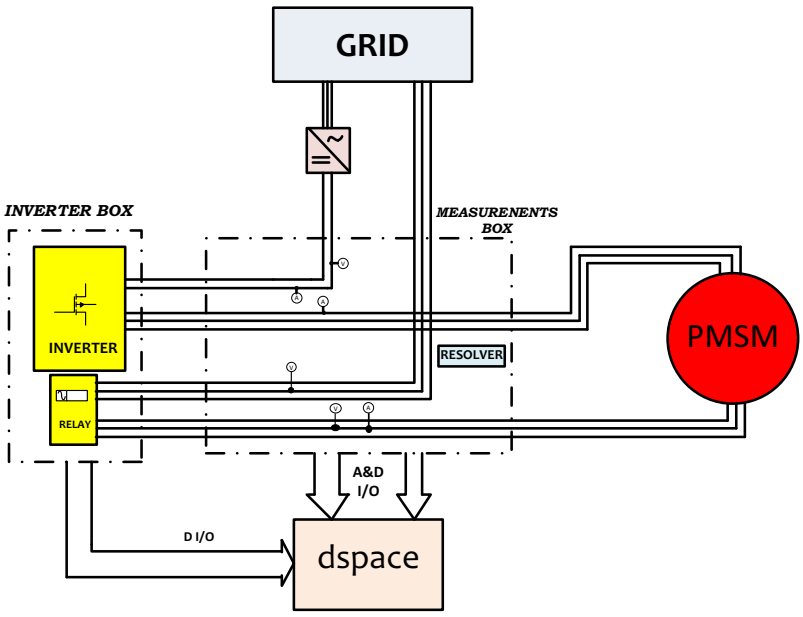

Figure 13 Schematic diagram of implemented drive system.

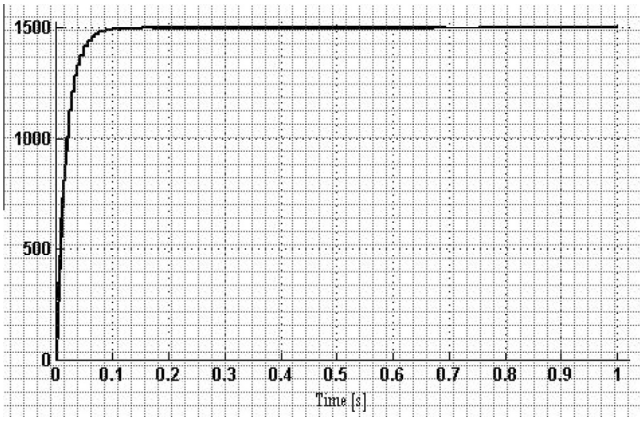

Figure 14 Experiment results: response of the speed of PMSM.

- A ±24 V DC voltage source that feeds the grid contactor.
- A four leg switch-mode inverter that uses MOSFET switches (one leg is spare).
- A relay (C3-A 30) for the PMSM secondary winding connection to the grid.
- A designed electronic board to drive the relay.

- The PMSM with double stator windings and the resolver already installed on the shaft. Resolver coils are available from the motor through a 12-pin connector installed in the motor housing.
- Control system is based on the dSpace, including the following parts:
  - Two CP1103 dSpace board with analog and digital I/O.
  - A CLP1103 dSpace board with luminous LEDs that show the state of the different signals.
  - The optocard that in case of over-current in inverter shuts down the PWM signal to the transistors of the inverter to avoid damaging the converter.
  - A DIO interface card that receives the measurement signals and sends an error signal to the optocard in case of over-currents.

The secondary winding voltages and currents are measured by the transducers. Moreover, there is a relay for connecting the three-phase grid voltages to the secondary set of windings. The machine used in the practical setup is a surface mounted PMSM. The motor parameters used in the practical setup are the same as those considered in the simulations. The magnetic flux created by the permanent magnets has a fixed value. For PMSM, the inductances in direct and quadrature axes are the same values.

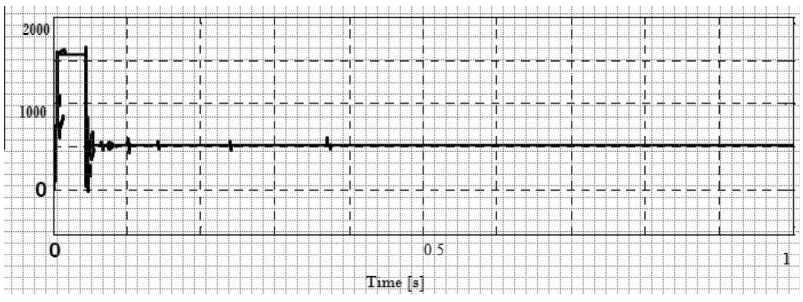

Figure 15 Experiment results: response of the power of PMSM.

Table A.1 Values of the parameters of the PMSM considered in the simulations.

Parameter	Value	Description
V_{DC}	300 V	DC voltage
ω_n	1500 rpm	Rated speed
R_s	0.4 Ω	Stator phase resistance
L_s	13 mH	Stator phase inductance
P	2	Pole pairs
T_n	3 N m	Rated torque
J	0.004 kg m^2	Inertia
B	0.002 N m/rad/s	Viscous coefficient

Figs. 14 and 15 show the experimental results of the implemented PMSM drive. As shown, noting to Fig. 4(c) and Fig. 6, the performance of the proposed control strategy in experiment is good.

6. Conclusion

In this paper, the direct power control (DPC) technique for controlling PMSM based on a neural network based speed estimator was presented. This proposed sensorless scheme was a new approach which employed a model reference adaptive system (MRAS) speed observer that used the current model as an adaptive model for DPC control PMSM drives. The nonlinear model of the motor was linearized based on quadratic linearization technique and removed the dominant quadratic nonlinearity of the model as well as higher order terms involving the input in the system. The simulations confirmed that the proposed control approach was able to control the PMSM for the linearized model as well as for the nonlinear model of the motor. The simulation and experimental results confirmed the effectiveness of this control strategy in tracking the reference power as well as reducing the ripples.

Appendix A

A.1. Parameters values

See Table A.1.

A.2. Linearized model of PMSM

The PMSM model can be written in the standard form as follows:

$$\dot{x} = Ax + Bu + f^2(x)$$

$$x = [\,x_1 \quad x_2 \quad x_3\,]^T, \quad u = [\,u_1 \quad u_2\,]^T, \quad f^2(x) = \begin{bmatrix} k_1 x_2 x_3 \\ k_2 x_3 x_1 \\ k_3 x_2 x_1 \end{bmatrix}$$

where $[\,x_1 \quad x_2 \quad x_3\,]^T = [\,i_d \quad i_q \quad \omega_e\,]^T$ is the state vector, and $[\,u_1 \quad u_2\,]^T = [\,v_{qs} \quad v_{ds}\,]^T$, and k_1, k_2, k_3 are constants defined in the literature. Applying the quadratic linearization theorem to this model, the linearized model of PMSM becomes

$$\varphi(x) = \varphi^{(2)}(x) = \begin{bmatrix} 0 \\ k_1 x_2 x_3 \\ k_1 x_3^2 \end{bmatrix}, \quad \alpha(x) = \begin{bmatrix} -k_3 x_2 x_1 \\ -k_2 x_3 x_1 \end{bmatrix}$$

$$\beta^{(m-1)}(x) = (-1)^{(m-1)} \left(B^T \frac{\partial \varphi^{(2)}(x)}{\partial x} B \right)^{(m-1)}, m \geqslant 2$$

Thus, the system can be reduced to

$$\dot{y} = Ay + Bv$$

References

[1] Lee Kwang-Woon, Park Sungin, Jeong Seongki. A seamless transition control of sensorless PMSM compressor drives for improving efficiency based on a dual-mode operation. IEEE Trans Power Electron 2015;30(3):1446–56.

[2] Banerjee Abhik, Mukherjee V, Ghoshal SP. Intelligent controller for load-tracking performance of an autonomous power system. Ain Shams Eng J 2014;5(4):1167–76.

[3] Behjat Vahid, Hamrahi Mehrdad. Dynamic modeling and performance evaluation of axial flux PMSG based wind turbine system with MPPT control. Ain Shams Eng J 2014;5(4):1157–66.

[4] Hu Jiefeng, Zhu Jianguo, Zhang Yongchang, Platt G. Predictive direct virtual torque and power control of doubly fed induction generators for fast and smooth grid synchronization and flexible power regulation. IEEE Trans Power Electron 2013;28 (7):3182–94.

[5] Casadei D, Serra G, Tani A. Implementation of a direct torque control algorithm for induction motors based on discrete space vector modulation. IEEE Trans Power Electron 2000;15 (4):769–77.

[6] Kazmierkowski MP, Krishnan R, Blaabjerg F. Control in power electronics-selected problems. Academic Press; 2002, ISBN 0-12-402772-5, ch.3.

[7] Rijcke SD, Ergun H, Van Hertem D, Driesen J. Grid impact of voltage control and reactive power support by wind turbines equipped with direct-drive synchronous machines. IEEE Trans Sustain Energy 2012;3(4):890–8.

[8] Tremblay E, Atayde S, Chandra A. Comparative study of control strategies for the doubly fed induction generator in wind energy conversion systems: a dsp-based implementation approach. IEEE Trans Sustain Energy 2011;2(3):288–99.

[9] Shuhui L, Haskew TA, Williams KA, Swatloski RP. Control of DFIG wind turbine with direct-current vector control configuration. IEEE Trans Sustain Energy 2012;3(1):1–11.

[10] Giraldo E, Garces A. An adaptive control strategy for a wind energy conversion system based on PWM-CSC and PMSG. IEEE Trans Power Syst 2014;29(3):1446–53.

[11] Muyeen SM, Takahashi R, Murata T, Tamura J. A variable speed wind turbine control strategy to meet wind farm grid code requirements. IEEE Trans Power Syst 2010;25(1):331–40.

[12] Genduso Fabio et al. Back-EMF sensorless control algorithm for high dynamics performances PMSM. IEEE Trans Indust Electron 2010;57(6):2092–100.

[13] Mohammadi J et al. A combined vector and direct power control for DFIG-based wind turbines. IEEE Trans Sustain Energy 2014;29(3):767–75.

[14] Chilipi RR, Singh B, Murthy SS. Performance of a self-excited induction generator with DSTATCOM-DTC drive-based voltage and frequency controller. IEEE Trans Energy Convers 2014;29 (3):545–57.

[15] Nian Heng, Song Yipeng. Direct power control of doubly fed induction generator under distorted grid voltage. IEEE Trans Power Electron 2014;29(2):894–905.

[16] Muljadi E, Singh M, Gevorgian V. Doubly fed induction generator in an offshore wind power plant operated at rated V/Hz. IEEE Trans Indust Appl 2013;49(5):2197–205.
[17] Castilla M et al. Direct rotor current-mode control improves the transient response of doubly fed induction generator-based wind turbines. IEEE Trans Energy Convers 2010;25(3):722–31.
[18] Zhang Yongchang, Hu Jiefeng, Zhu Jianguo. Three-vectors-based predictive direct power control of the doubly fed induction generator for wind energy applications. IEEE Trans Power Electron 2014;29(7):3485–500.
[19] Santos-Martin D et al. Dynamic programming power control for doubly fed induction generators. IEEE Trans Power Electron 2008;23(5):2337–45.
[20] Zhou Peng, He Yikang, Sun Dan. Improved direct power control of a DFIG-based wind turbine during network unbalance. IEEE Trans Power Electron 2009;24(11):2465–74.
[21] Krause PC. Analysis of electric machinery. New York: McGraw-Hill; 1987.
[22] Qin S, Xue X. A two-layer recurrent neural network for non-smooth convex optimization problems. Trans Neural Networks Learn Syst 2014;26(6):1149–60.
[23] Rumelhart D, McClelland J. Parallel distributed processing. Cambridge, Mass: MIT Press; 1986.
[24] The Mathworks, MATLAB/SIMULINK, R2013b, Version 8.2.0.701.
[25] Bose Bimal K. Modern power electronics and AC drives. Pearson Education, Inc.; 2002.
[26] Parvathy AK. Rajan Aruna, Devanathan R. Linearization of PM synchronous motor model. Technical Report, Department of EEE, Hindustan College of Engineering, Tamil Nadu; May 2005.
[27] Parvathy AK, Rajan Aruna, Devanathan R. Complete quadratic linearization of PM synchronous motor model. In: The proceedings of NPEC; 2005. p 49–52.

Mahdi Zolfaghari was born in Aleshtar, Lorestan, Iran, in 1987. He received his M.Sc. degree in electrical engineering from Department of Electrical Engineering, Feiz Institute of Higher Education, Kashan, Iran, in 2013. He is a member of Iranian Inventors Association (IIA). Currently, he is a Ph.D. student in electrical engineering at department of electrical engineering, Amirkabir University of Technology (Tehran Polytechnic), Tehran, Iran. His current research interests include smart grids, renewable energy, power system optimization, robust control and uncertain systems analysis, fuzzy expert systems, artificial neural networks, electrical machines and drive systems, and soft computing.

Seyed Abbas Taher was born in Kashan, Isfahan, Iran, in 1964. He received his B.Sc. degree in electrical engineering from Amirkabir University of Technology, Tehran, Iran, in 1988 and his M.Sc. and Ph.D. degrees in electrical engineering from Tarbiat Modares University, Tehran, Iran, in 1991 and 1997, respectively. In 1996, he joined Faculty of Engineering, University of Kashan, in which he has been an associate professor since 2009. His current research interests include power system optimization and control design, analysis of electrical machines, power quality, and renewable energy.

David Vindel Munuz was born in Madrid, Spain. He received his B.Sc. degree in electrical engineering from the Universidad Carlos III de Madrid, Spain, in 2010 and his M.Sc. degree in electrical engineering from the Chalmers University, Sweden, in 2011. Currently, he is a subcontract engineer in SENER INGENIERIA Y SISTEMAS, Madrid, Spain. His research interests include design, simulation & implementation of PMSM electric drive, and electricity for hybrid vehicles.